Tellus (2004), 56A, 154–166
Printed in UK. All rights reserved

TELLUS

Effects of solar irradiance forcing on the ocean circulation and sea-ice in the North Atlantic in an isopycnic coordinate ocean general circulation model

By ODD HELGE OTTERÅ[1,2,*] and HELGE DRANGE[1,2,3], [1]*Nansen Environmental and Remote Sensing Center, Edv. Griegsvei 3A, 5059 Bergen, Norway;* [2]*Bjerknes Centre for Climate Research, Allégt. 55, 5007 Bergen, Norway;* [3]*Geophysical Institute, University of Bergen, Allégt. 70, 5007 Bergen, Norway*

(Manuscript received 25 April 2003; in final form 15 October 2003)

ABSTRACT

The sensitivity of the ocean circulation to changes in solar irradiance is examined using an isopycnic coordinate, global ocean general circulation model (OGCM) coupled to a thermodynamic/dynamic sea-ice model. In the experiments, changes in the surface radiation forcing are calculated based on orbital data assuming that the atmospheric conditions are otherwise unchanged. Two sensitivity experiments are run with the ocean–sea-ice model: one with high and one with low solar irradiance representative of the last interglacial and glacial periods, respectively. The results show that the Atlantic merdional overturning circulation (AMOC) is increased (reduced) in response to lower (higher) summer solar irradiance. It is found that changes in the Arctic sea-ice volume and area are the main reason for the response. For the low solar irradiance case, less sea-ice is melted in summer leading to a saltier Arctic Ocean. This saltier water is then advected into the sinking regions in the winter, enhancing the intermediate and deep water formation. For the high solar irradiance case, a similar, but opposite, response occurs. The results thus confirm that the AMOC is very sensitive to external forcing. It is suggested that the scheme used for calculating changes in solar irradiance could prove useful when conducting glacial inception studies with fully coupled atmosphere–ocean models.

1. Introduction

An important climatic change occurred during the transition from the Eemian interglacial to the beginning of the last glacial between 120–115 kyr BP (kyr BP is 1000 yr before present). The shifts between interglacial and glacial climate regimes are caused by processes involving orbital forcing (the Milankovitch mechanism) and biogeochemical cycles. However, changes in the solar radiation and its geographical and seasonal distribution cannot alone explain the observed glaciation cycles (Crowley and North, 1991). Therefore, positive feedbacks in the climate system must also have acted as important amplifiers to the external forcing (Broecker and Denton, 1990). One important mechanism involves the inland ice sheets (Imbrie et al., 1992). As the summer insolation decreases to values low enough to prevent snowmelt over large areas during summer, the ice–albedo feedback aids the glaciation process (Budyko, 1969). It has also been suggested that sea-ice feedbacks may act as climate switches and may participate in shaping some of the features of the observed past climate variability (Gildor and Tziperman, 2001).

Another mechanism involves the deepwater formation in the northern North Atlantic and in the Nordic Seas. It is generally believed that formation of deepwater is an important driving mechanism for the AMOC (Broecker, 1991). In these regions, relatively small perturbations in the sea surface salinity can enhance or weaken deep mixing, and thereby change the general circulation (Rahmstorf, 1999).

The role of the AMOC during the last glacial inception is not clear. In the northwestern Atlantic, southeast of Newfoundland, analyses of a deep-sea core (CH69-K09) show that δ^{13}C in benthic foraminifera increased during the period of rising benthic δ^{18}O values at the transition from stage 5e to stage 5d (Labeyrie et al., 1999). This indicates increased strength of the AMOC during the growth of ice sheets. This view has also found some support in climate modelling studies (Wang and Mysak, 2000; Meissner and Gerdes, 2002).

However, Khodri et al. (2001) find a reduced AMOC in their coupled ocean–atmosphere simulation with solar insolation representing the orbital parameters at 115 kyr BP. The principal mechanism operating in this simulation is an enhanced

*Corresponding author.
e-mail: oddho@nersc.no

meridional atmospheric moisture transport leading to build-up of perennial snow over Canada, a weaker Icelandic low, and a cooling of the high northern latitudes. These findings are in general agreement with observations of a cooling in the Nordic Seas before the major ice sheets developed (Cortijo et al., 1994; Fronval and Jansen, 1996). Cooler conditions in high northern latitudes are not necessarily inconsistent with a stronger AMOC. For instance, location of the major deepwater formation sites south of the Greenland–Scotland ridge could explain a cooling in the Nordic Seas while the subpolar North Atlantic would stay warm and saline (Meissner and Gerdes, 2002).

There are thus a number of possible feedback mechanisms between the atmosphere, sea ice and ocean during the inception (or termination) of glaciations. As a first step to model aspects of the ocean circulation during the last glacial inception, we present a simple sensitivity experiment using a global OGCM coupled to a dynamic and thermodynamic sea-ice model. In this study, we examine the transient response of the modelled ocean regime to changes in the summer irradiance at high latitudes. The changes in surface radiation forcing are calculated based on the orbital data of Berger and Loutre (1991) using the scheme of Kutzbach and Gallimore (1988) and by assuming that the atmospheric conditions are otherwise unchanged. Three experiments are performed: one experiment with high summer insolation (i.e. interglacial conditions representing 125 kyr BP, hereafter W125), one experiment with low summer insolation (i.e. glacial inception representing 115 kyr BP, hereafter C115), and one experiment with present-day radiation forcing (CTRL).

It is important to note that no atmospheric feedbacks are involved in the model runs presented here. Therefore, the results should be viewed as a sensitivity study of the ocean circulation to solar irradiance only, rather than a comprehensive study of the glacial inception. However, the results provide a useful test of the scheme used for calculating solar irradiance changes, and will be extended to fully coupled atmosphere–ocean models in the future.

The paper is organized as follows. In Section 2 the coupled ocean–sea-ice model is introduced, and the design of the experiment is described. In Section 3 we present the results from the model simulations. Finally, in Section 4 the results are discussed and some concluding remarks are given.

2. The coupled ocean–sea-ice model

2.1. General features

The model system used in this study consists of the Miami isopycnic coordinate ocean model (Bleck et al., 1992), a sea-ice module consisting of the Hibler (1979) rheology in the implementation of Harder (1996), and the thermodynamics of Drange and Simonsen (1996). The model is configured with a local horizontal orthogonal grid system with the poles located over North America and over Eurasia (Bentsen et al., 1999), yielding a moderate horizontal resolution in the northern North Atlantic of about 80 km (Fig. 1).

The OGCM is configured with 26 layers in the vertical, with the uppermost mixed layer (ML) having a temporal and spatial varying density. The densities (in σ_0 units) of the subsurface isopycnic layers are 23.54, 24.12, 24.70, 25.28, 25.77, 26.18, 26.52, 26.80, 27.03, 27.22, 27.38, 27.52, 27.63, 27.71, 27.77, 27.82, 27.86, 27.90, 27.94, 27.98, 28.01, 28.04, 28.07, 28.10, 28.85 and 29.10. The listed densities are chosen to ensure a proper representation of the major water masses in the North Atlantic/Nordic Seas region.

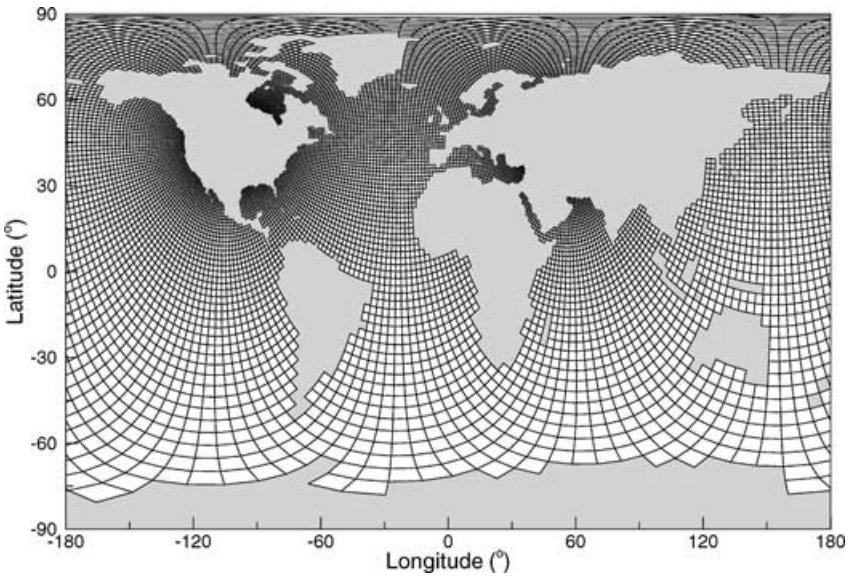

Fig. 1. The horizontal grid mesh configuration applied in the experiments.

The vertically homogeneous ML utilizes the Gaspar et al. (1990) bulk parametrization for the dissipation of turbulent kinetic energy, and has temperature, salinity and layer thickness as prognostic variables. In the subsurface layers, temperature and layer thickness are the prognostic variables, while salinity is diagnosed from a simplified equation of state (Friedrich and Levitus, 1972). The bathymetry is computed for each grid box as the arithmetic mean value of the ETOPO-5 data base (NOAA, 1988).

2.2. Spin-up integration and forcing

For the spin-up integration, the model was initialized with January Levitus and Boyer (1994) and Levitus et al. (1994) climatological temperature and salinity fields, respectively, a 2-m thick sea-ice cover based on the climatological sea-ice extent (Gloersen et al., 1992), and an ocean at rest. The model was then integrated for 420 yr by applying the monthly mean National Center for Environmental Prediction/National Center for Atmospheric Research (NCEP/NCAR) atmospheric wind stress, short wave, long wave, latent and sensible heat fluxes, precipitation, runoff and sea level pressure fields. The momentum, heat and freshwater fluxes are modified when the modelled surface state differs from the NCEP/NCAR reanalysis surface state by the Fairall et al. (1996) bulk parametrization scheme (Bentsen and Drange, 2000).

During the spin-up period, the ML temperature and salinity were relaxed towards the monthly mean climatological values of Levitus and Boyer (1994) and Levitus et al. (1994), respectively. The e-folding relaxation time-scale was set to 30 d for a 50-m thick ML, and it was reduced linearly with ML thicknesses exceeding 50 m. No relaxation was applied in waters where sea ice is present in March in the Arctic, and in September in the Antarctic, to avoid relaxation towards temperature or salinity outliers in the poorly sampled polar regions. In addition, the relaxation was limited to a maximum model-to-observation mismatch of 0.5 psu and 1.5 °C for salinity and temperature, respectively. This restriction is especially important in the Atlantic Ocean, as it tends to maintain the simulated hydrodynamic properties of the water masses associated with the Gulf Stream–Labrador Sea system regardless of the actual position of these current systems. The runoff is included by adding the freshwater into the appropriate coastal grid cells using the scheme described in Bentsen (2002).

For years 400–420 of the spin-up integration, the mean weekly freshwater relaxation fluxes were diagnosed and stored. For a further 80-yr integration, and for the three model experiments started from year 500 of the spin-up integration, the temperature relaxation was switched off. The salinity relaxation was reduced by increasing the relaxation time-scale from 30 d to 2 yr. In addition, the diagnosed freshwater fluxes were added to the ML. The use of weak relaxation of salinity and the diagnosed freshwater fluxes ensures that the strength of the AMOC remains fairly stable in CTRL, and that temperature and salinity anomalies are free to develop, propagate and decay in the sensitivity experiments.

Although it is clear that only a fully coupled ocean–atmosphere GCM can represent the ocean–atmosphere interaction in the climate system, the use of mixed boundary conditions has been widely applied in climate simulations with OGCMs. It is a common finding that in global OGCMs driven with mixed boundary conditions, the AMOC may be too sensitive to buoyancy perturbations (Mikolajewicz and Maier-Reimer, 1994). The possibility that this is the case for the model experiments presented here can only be evaluated from similar experiments performed with fully coupled climate models, which is beyond the scope of the paper.

2.3. Set-up of the sensitivity experiments

The hypothesis has been made that the Nordic Seas form the initial response to insolation forcing, translating the insolation forcing to the rest of the climate system via the albedo feedback and reduced thermohaline overturning (Imbrie et al., 1992). Motivated by this, the sensitivity of the ocean circulation to changes in the summer solar insolation at high latitudes (60°N) is examined.

To simulate the extreme high and low values in high latitude summer insolation, the orbital parameters (eccentricity, obliquity and perihelion) are set at the values for 125 and 115 kyr BP, respectively (Table 1). In order for the heat fluxes in the sensitivity experiments to be consistent with CTRL, the downward solar irradiance from the NCEP/NCAR data have been used for all experiments. Therefore, for the sensitivity experiments the NCEP/NCAR downward solar irradiance is modified by a latitude–time-dependent factor S_{fac} according to

$$S_{\mathrm{fac}} = \frac{S_{\mathrm{x}}}{S_{\mathrm{pres}}}.$$

Here S_{pres} and S_{x} are the solar insolation calculated using the scheme of Kutzbach and Gallimore (1988) for the present-day situation and for the sensitivity experiments, respectively. Using this factor gives about a 6% (10–12%) decrease (increase) in summer solar irradiance at 60°N at 115 kyr BP (125 kyr BP) compared to the present-day situation (Fig. 2). In CTRL, $S_{\mathrm{fac}} = 1$, implying that no changes were made to the NCEP solar irradiance.

Table 1. *The orbital parameters (Berger and Loutre, 1991) used for calculating the incoming solar radiation at the top of the atmosphere for CTRL, C115 and W125, respectively.*

	Control	115 kyr BP	125 kyr BP
Eccentricity	0.016724	0.041421	0.040013
Obliquity	23.446	22.405	23.798
Perihelion-180°	102.04	110.88	307.14

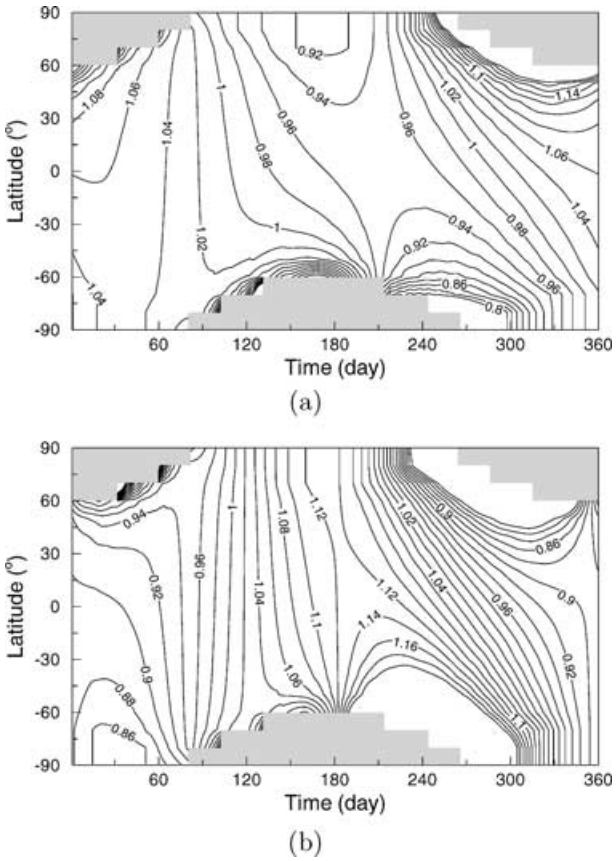

Fig. 2. The factor S_{fac} described in the text plotted as a function of latitude and time of year for (a) C115 and (b) W125. Contour interval is 0.02.

3. Results

3.1. Sea-ice response

The evolution of Arctic ice volume shows that the ice volume is fairly stable at about 28 500 km^3 in CTRL (Fig. 3a), and in general agreement with model studies of the present-day climate state (Hilmer and Lemke, 2000). The integrated Arctic sea-ice area varies in the model from 6.4 $\times$ 10^6 km^2 in summer to 13.9 $\times$ 10^6 km^2 in winter (Figs 3b and c), in good agreement with the observed values of 6.2 $\times$ 10^6 km^2 and 13.9 $\times$ 10^6 km^2, respectively (Gloersen et al., 1992). Furthermore, the horizontal distribution of the sea-ice in years 31–60 shows that the ice edge is well simulated by the model in both summer and winter (Figs 4a and b), except for a slight underestimation of the sea-ice extent in the Labrador Sea.

In C115, the ice volume increases by about 6000 km^3 during the 90-yr integration period, while in W125 a slightly smaller decrease of about 4000 km^3 is obtained (Fig. 3a). As for the Arctic sea-ice cover, the most noticeable changes occur in September which is to be expected because the largest changes in the solar irradiance occur in summer (Fig. 2). In C115, the Arctic sea-ice area increases by about 600 000 km^2, while a 400 000-km^2 decrease can be found in W125 (Fig. 3b). For March, the changes in the sea-ice area are not significant (Fig. 3c). The pronounced episodic reductions in the winter sea-ice area are

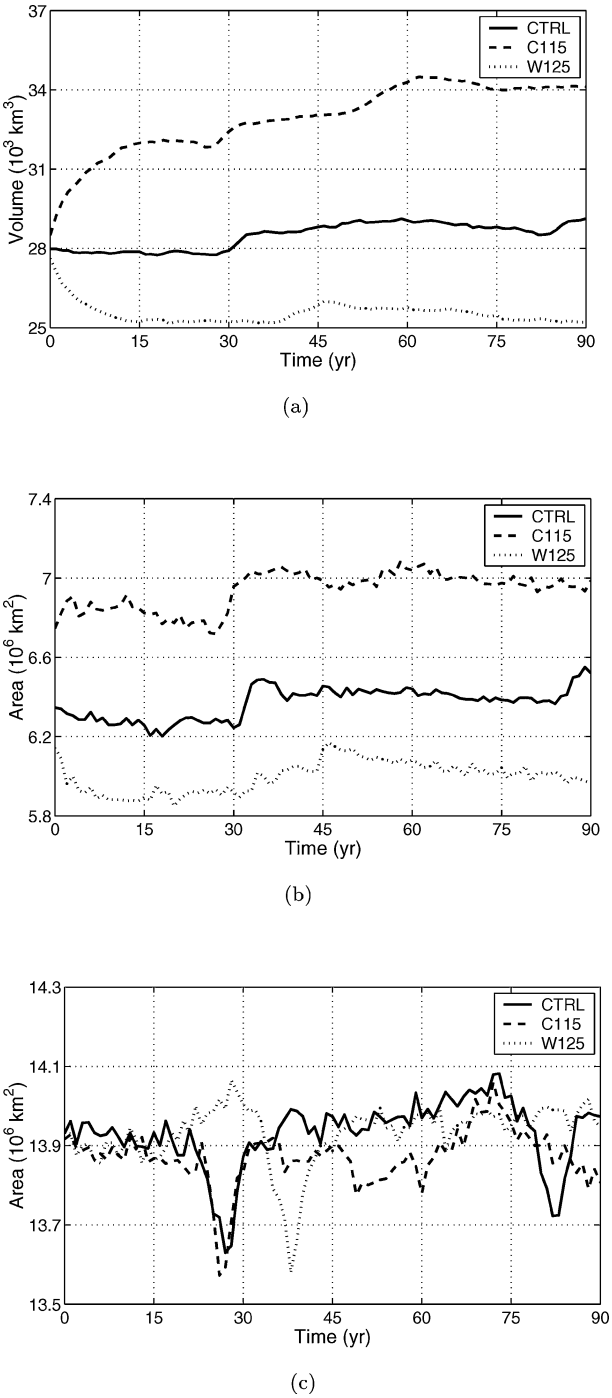

Fig. 3. Time series of (a) the annual mean sea-ice volume (km^3) in the Arctic, and the Arctic sea-ice area (km^2) in (b) September and (c) March for CTRL (solid line), C115 (dashed line) and W125 (dotted line).

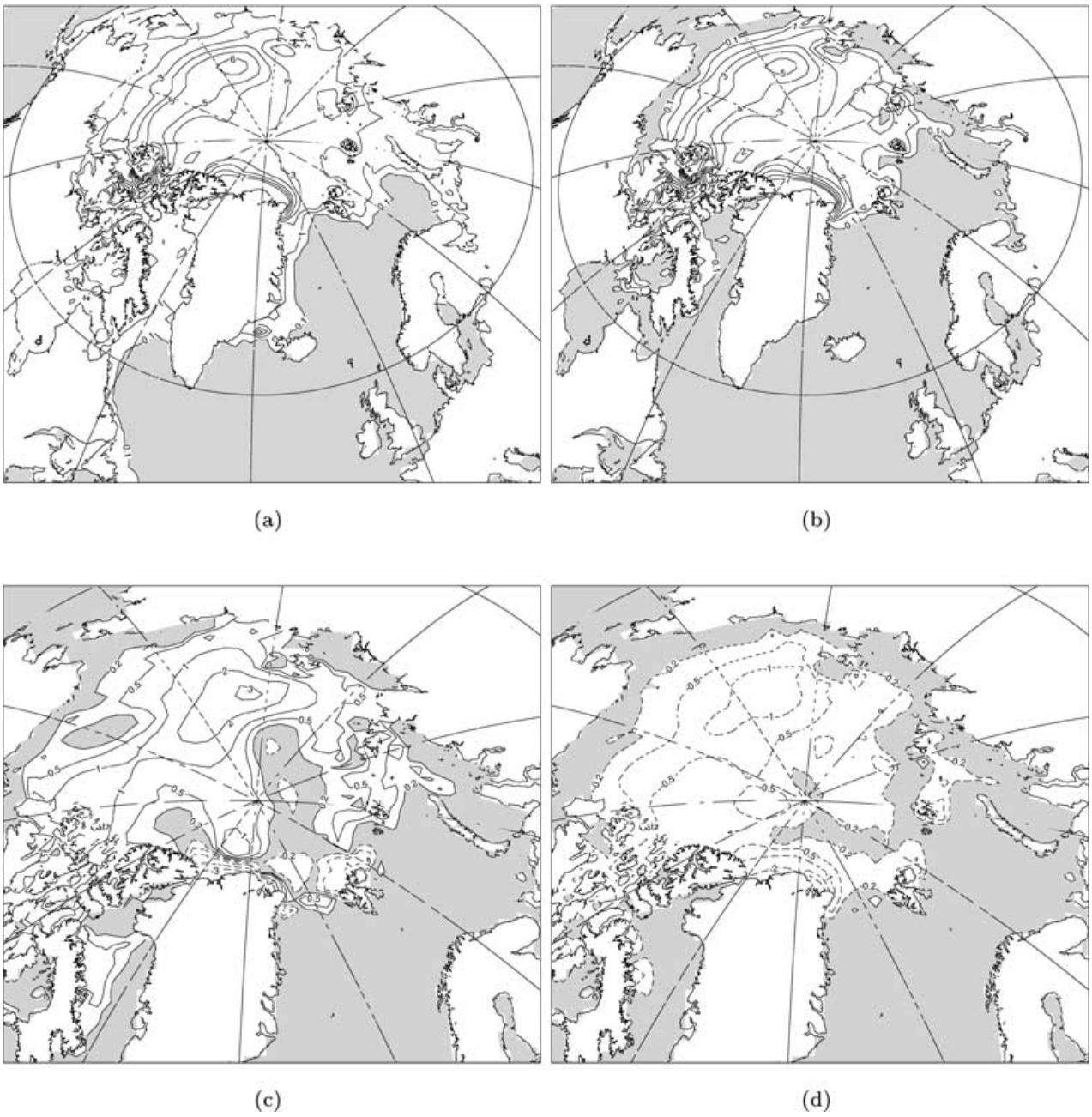

Fig. 4. Averaged sea-ice thickness (m) for years 31–60: (a) March in CTRL; (b) September in CTRL; (c) C115-CTRL in September; (d) W125-CTRL in September. Contour intervals are 1 m. In addition, the 0.1-m contour isoline is shown in (a) and (b) and the 0.2-m and 0.5-m contour isolines are shown in (c) and (d).

caused by melting of ice in Baffin Bay, and are discussed below.

Figures 4c and d present the spatial distribution of Arctic sea-ice anomalies from C115 and W125 for September averaged over years 31–60. The pattern for March is similar for both cases and is therefore not shown. In C115, positive anomalies cover most of the Arctic Ocean, with the largest increases in the ice thickness (1–3 m) found in a belt extending from the Canadian Archipelago across the Canadian Basin (Fig. 4c). The changes are more profound in the Canadian Basin than in the Eurasian Basin.

In W125, the sea-ice thickness is reduced over most of the Arctic Ocean (Fig. 4d). The most noticeable changes occur in the Canadian Basin and in a region north of the Greenland coast, with a reduction in ice thickness in excess of 1 m.

3.2. General surface circulation

The circulation field for the Atlantic–Arctic region is, in general, in accordance with observations (Fig. 5). The most pronounced exception is the too northerly separation of the Gulf Stream (GS) off the North American coast. This is a classical problem for OGCMs; a properly resolved GS requires a horizontal resolution one order of magnitude higher than in the present study (Bleck et al., 1995). A consequence of the too northerly separation of the GS is that the Atlantic Water (AW) entering the Nordic Seas is too cold.

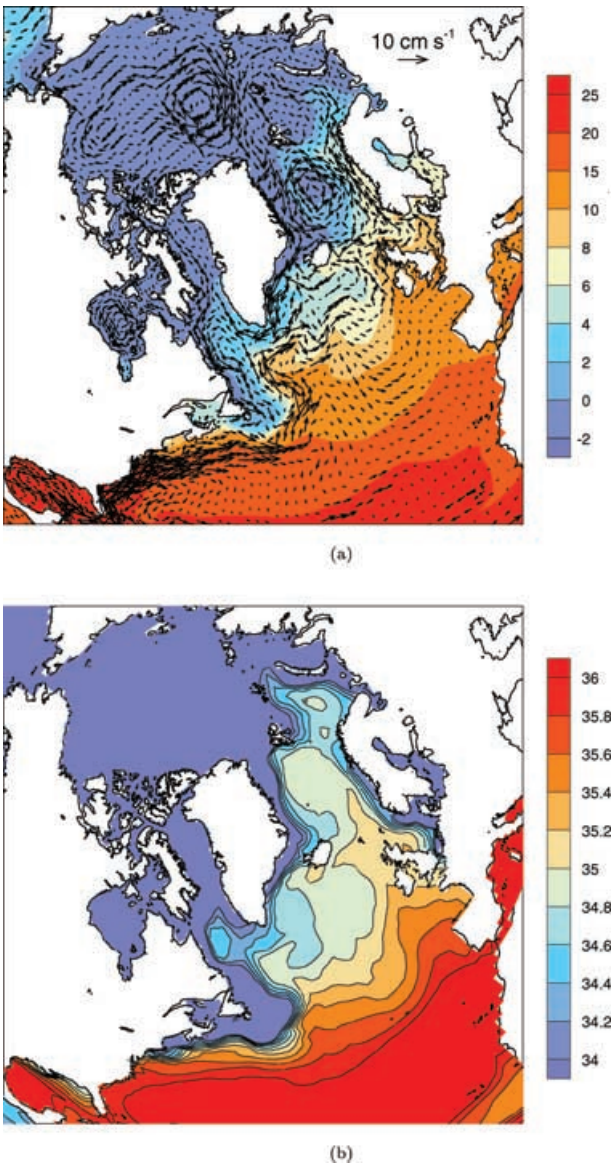

Fig. 5. Annual mean values for years 31–60 in CTRL of (a) temperature (°C) and velocity (cm s^{-1}), and (b) salinity (psu). All values are are averaged over the upper 100 m of the water column. A reference vector is provided in the upper-right part of (a).

In the western part of the northern North Atlantic, some of the warm and saline water masses are seen to enter the subpolar gyre where they eventually are brought into the sinking regions in the Irminger and Labrador Seas. The relatively high salinity of these waters combined with winter cooling is important for the formation of intermediate and deep water masses in these regions.

In the Arctic Ocean, the general surface circulation is dominated by the Beaufort Gyre and the Transpolar Drift (TD). The cold and fresh Polar Water leaves the Arctic via the East Greenland Current (EGC), and continues southward along the coast of Greenland. Most of the Polar Water flows through the Denmark Strait and enters the subpolar gyre. However, a branch of the cold and fresh Arctic water continues north of Iceland and is trapped in the cyclonic circulation in the Nordic Seas.

In C115, an increase in the annual mean temperature over the upper 100 m along the GS and in the subpolar gyre of the northwestern North Atlantic is obtained (Fig. 6a). In the central part of the northern North Atlantic, there is a general cooling, most likely due to the reduced solar irradiance in summer. Furthermore, an intensification of the GS along the North American continent can also be seen. In the Nordic Seas, only minor changes are found. The C115 integration is further characterized by positive salinity anomalies in large parts of the Arctic Ocean in years 31–60 (Fig. 6c). The only exceptions are the East Siberian Sea, the Eurasian Basin and the Kara Sea. Positive anomalies appear to be transported into the sinking regions of the Irminger and Labrador Seas through the Fram Strait and the Canadian Archipelago. Furthermore, positive anomalies are also found south of Newfoundland as more salt is transported northward with the intensified GS. In the Nordic Seas, a freshening in the western part is evident, linked to increased sea-ice transport through the Fram Strait. This increase is the result of a stronger and more southeastward shifted TD in C115 (not shown). This is also the reason for the reduced sea-ice thickness along the northern coast of Greenland (Fig. 4c), as a stronger and more southeastward directed TD leads to less accumulation of sea ice in this region.

In W125, cooling of the surface waters is obtained along a slightly weaker GS and in large parts of the subpolar gyre (Fig. 6b). However, the rest of the northern North Atlantic between 50–60°N is mostly characterized by a warming, presumably from enhanced solar irradiance in summer. Slightly higher surface temperatures in the Greenland Sea are also found. The changes in salinity in W125 show a freshening in most parts of the Arctic Ocean except for the Eurasian Basin (Fig. 6d). The negative anomalies are transported through the Fram Strait via the EGC and into the sinking regions in the Irminger and Labrador Sea. Along the GS and in most parts of the northern North Atlantic a freshening is obtained. In the Nordic Seas, no significant changes are found except slightly increased salinities in the western part due to reduced sea-ice export through the Fram Strait (not shown).

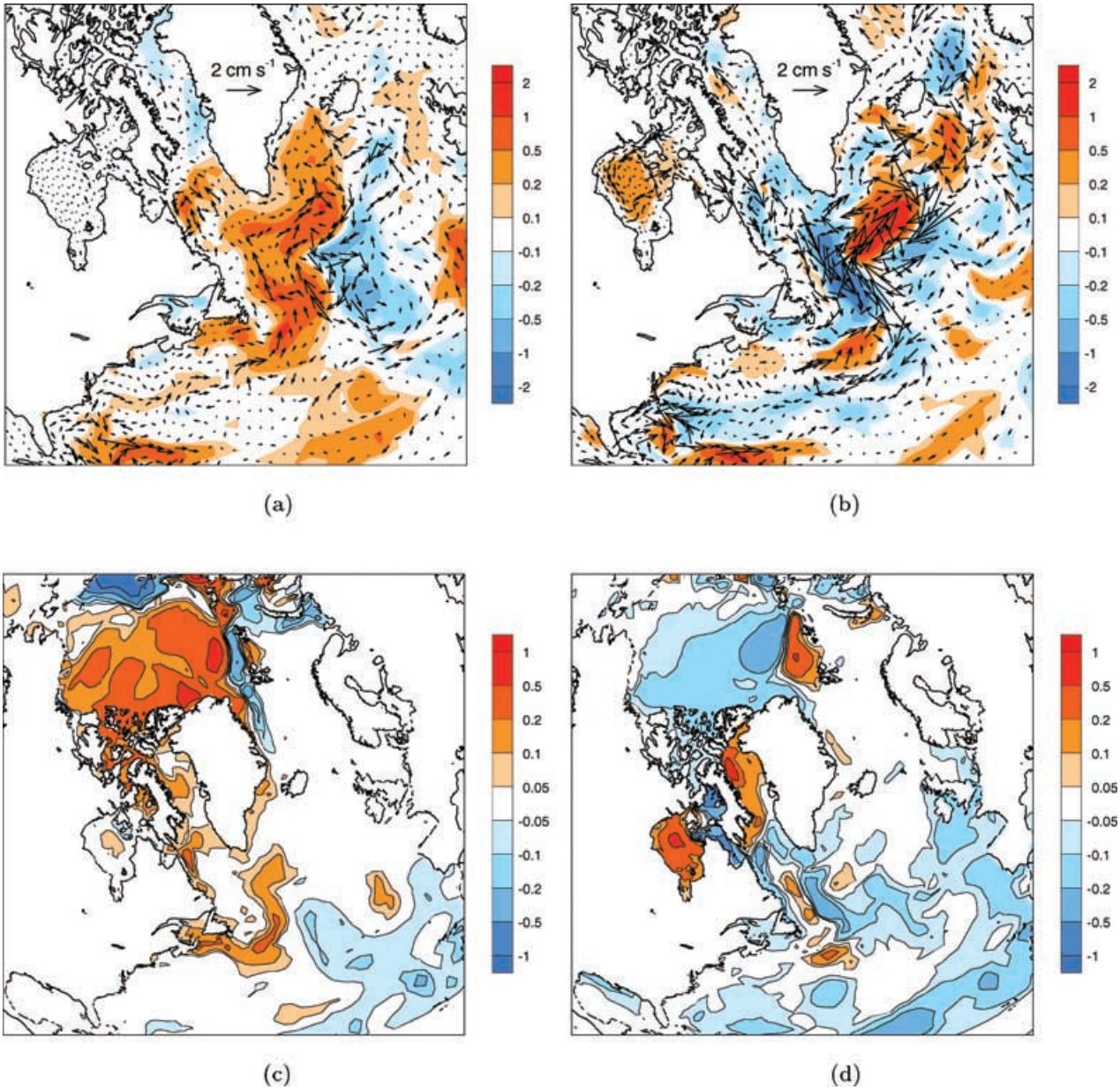

Fig. 6. Changes in the annual mean temperature (°C) and velocity (cm s^{-1}) for (a) C115−CTRL and (b) W125−CTRL. Changes in the annual mean salinity (psu) for (c) C115−CTRL and (d) W125−CTRL. All values are averaged over the upper 100 m of the water column. A reference vector is provided in the upper part of (a) and (b).

A rather peculiar feature in W125 is related to the positive salt anomalies in Baffin Bay in years 31–60 (Fig. 6d). Time series of the upper 100-m salinity in the Baffin Bay region show two distinct salinity pulses in CTRL: one peaking around year 28 and a second around year 83 (Fig. 7). The salinity anomalies are accompanied by minima in the ice volume in the region. The anomalies are caused by the intrusion of relatively warm and saline waters through the Davis Strait, thereby increasing the density of the ML. As the thickness of the ML increases, more warm and saline water masses are entrained into the ML from below, causing the sea ice to melt. The following decrease in the northward flow through the Davis Strait leads to a freshening of the ML and subsequent sea-ice formation. It is not clear whether or not this variability is part of some internal oscillation in the ocean–sea-ice system in the region or just a model artefact. In W125, the same mechanism operates, with the only difference being the timing of the AW intrusion across the Davis Strait. In W125, this intrusion occurs around year 40 leading to a peak in

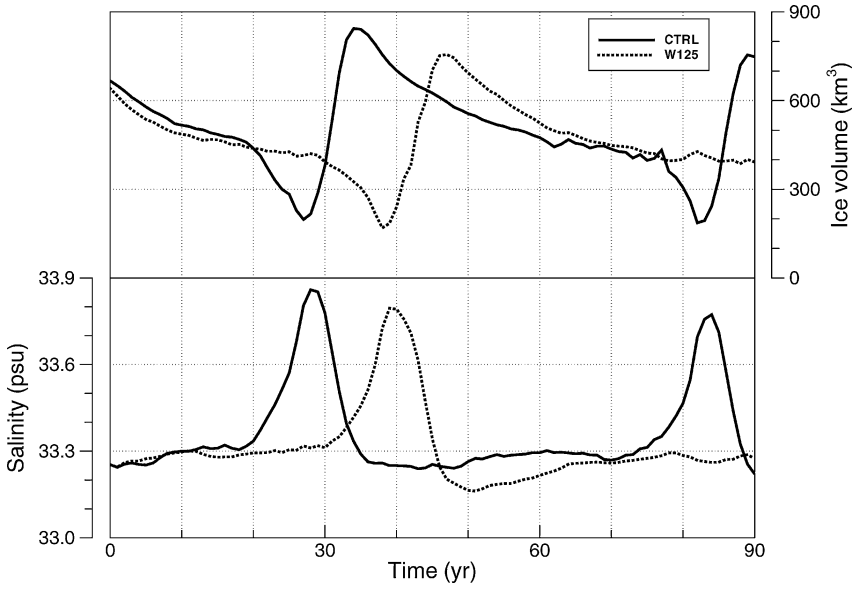

Fig. 7. Time series of the salinity (psu, lower panel) and sea-ice volume (km^3, upper panel) for Baffin Bay averaged over the upper 100 m of the water column in CTRL (solid line) and W125 (dotted line).

the surface salinity in the Baffin Bay region, which is reflected in Fig. 6d.

3.3. Winter mixing and AMOC responses

Volume mixing indices are constructed from the mean February to April (FMA) ML volume below 300 m in the areas where the FMA ML depth exceeds 1000 m at least once during the CTRL, C115 and W125 integrations (Fig. 8). In C115, the ML volume is increased in the subpolar seas over the first 60 yr, with the most noticeable changes taking place between years 31–60 (Fig. 9a). A rapid drop in the ML volume is found over the following 15 yr and a subsequent recovery towards the end of the period. In the W125 run, the ML volume is reduced over the whole integration. In the Nordic Seas, the changes in the ML volume are relatively small compared to the subpolar seas (Fig. 9b).

The spatial distribution of the changes in the ML thickness is shown in Fig. 10. In C115, an increased ML thickness of about 200 m is seen in the western part of the Labrador Sea for years 31–60, indicating enhanced winter mixing (Fig. 10a). In the Irminger Sea, the ML thickness is reduced in the northern part while slightly increased in the southern part. Interestingly, there is also increased mixing intensity south of Iceland indicating a slight shift in the convective activity southeastwards from the Irminger Sea. In the Nordic Seas, the only significant change is a reduced ML thickness in the western part, most likely because of increased freshwater transport via the Fram Strait. This leads to freshening of the ML here (Fig. 6c), and therefore suppressed deep mixing. In W125, the most prominent feature is a widespread 200-m reduction in the ML thickness in the Labrador

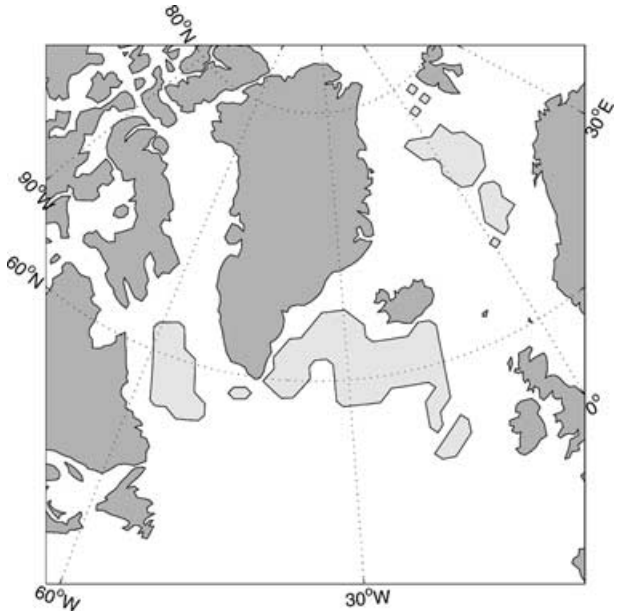

Fig. 8. The shading shows the regions in the North Atlantic and the Nordic Seas where the February–April ML depth exceeds 1000 m at least once in one of CTRL, C115 and W125 during the 90-yr integration period.

and Irminger Seas (Fig. 10b). In the Nordic Seas, the changes are generally small (less than 50 m).

The meridional structures of the AMOC stream function for CTRL, C115 and W125 for years 31–60 are displayed in Fig. 11. The AMOC in CTRL is characterized by northward flow close to the surface, sinking at high latitudes and a southward flow at greater depths (Fig. 11a). Due to the choice of reference pressure

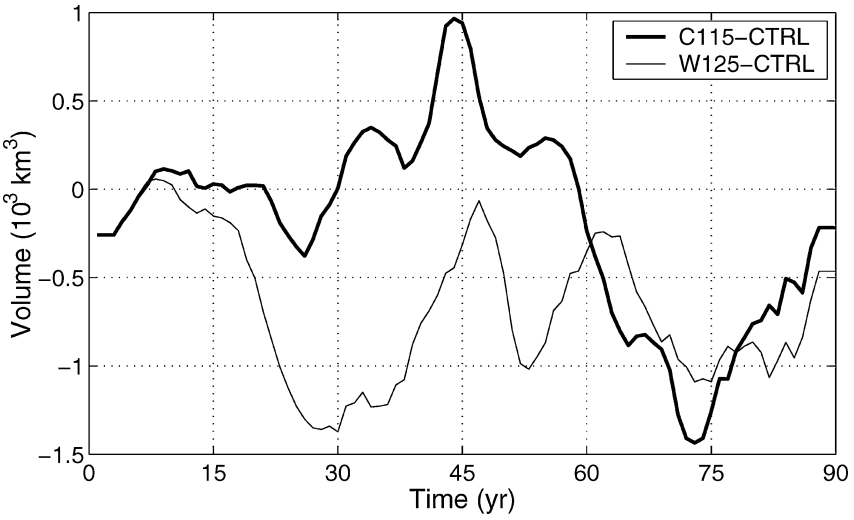

(a)

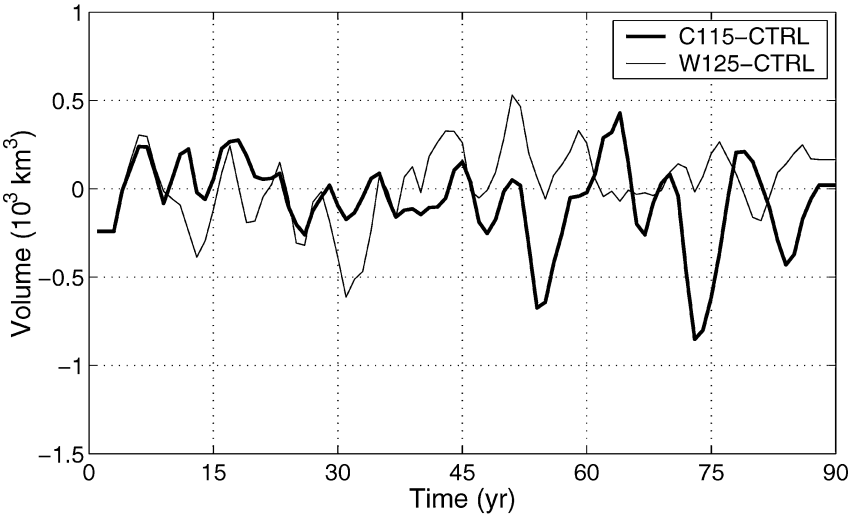

(b)

Fig. 9. Time series of the changes in the mean volume (km^3) of the ML water below 300 m (a) in the North Atlantic subpolar region and (b) in the Nordic Seas for C115–⟨CTRL⟩ (thick line) and W125–⟨CTRL⟩ (thin line). Here ⟨CTRL⟩ is the second-order polynomial least-squares fit to the 90-yr CTRL integration. The location of the mixing regions is provided in Fig. 8.

at the surface, the model is not able to represent the penetration of Antarctic bottom water. The small negative overturning values near the bottom match the mean volume transport of about 1 Sv through the Bering Strait. The strength of the AMOC is fairly stable throughout CTRL, varying between 16–18 Sv with a mean of about 17.5 Sv (not shown). This is in the range of 15 coupled models studied in Lambert and Boer (2001).

In C115, the meridional overturning circulation is enhanced by 0.5–1 Sv at mid-latitudes for years 31–60 (Fig. 11b). At the equator, an increase in the overturning of about 3 Sv is found at depths of about 3000 m. In W125, the meridional overturning circulation is reduced throughout the Atlantic, with a reduction of up to 2 Sv at 2000 m depths at 40°N (Fig. 11c).

4. Discussion

An important result of the presented simulations is the ∼3 Sv difference in the strength of the AMOC between the cold (C115) and warm (W125) integrations, with the cold state producing the strongest AMOC (Fig. 11). The mechanism responsible for this is related to changes in the Arctic sea-ice cover and volume (Figs 3 and 4). In C115, the solar irradiance at high latitudes in summer is reduced, leading to the expansion of Arctic sea-ice. Similarly, the sea-ice retreats under increased solar irradiance in W125. Reduced melting of sea-ice in summer in C115 has a strong impact on the sea surface salinities in the Arctic region, leading to increased salinities here (Fig. 6c). These

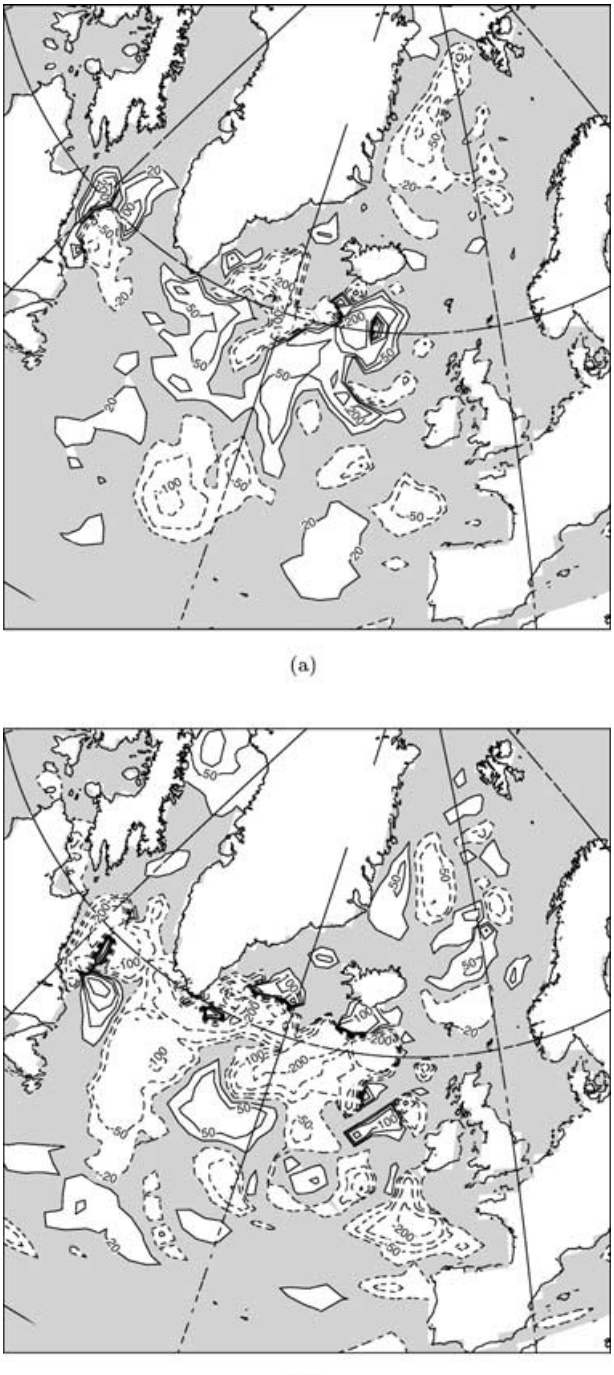

Fig. 10. Changes in the average ML thickness for March in years 31–60: (a) C115–CTRL and (b) W125–CTRL. Negative values indicate reduced ML thickness. Contour interval is 100 m. In addition, the 20-m and 50-m contour isolines are shown.

positive salinity anomalies are then transported through the Canadian Archipelago and Fram Strait into the sinking regions of the subpolar Atlantic, leading to enhanced intermediate and deep mixing here (Fig. 9a). This in turn intensifies the AMOC, leading to enhanced northward transport of AW with the GS system (Fig. 6a).

The stronger AMOC in C115 compared to W125 bears some resemblance to the model results of Meissner and Gerdes (2002), who modelled the glacial inception using a coupled ocean–atmosphere–sea-ice model. By storing part of the precipitation over continents within continental ice sheets, they simulated the build-up of ice sheets over land. This leads to reduced continental runoff, and in turn to an enhanced AMOC. In our simulations, the reason for the intensification is not linked to changes in the runoff, but rather to reduced freshwater fluxes from sea-ice melting.

Wang and Mysak (2000) simulated the initiation of glaciation using a coupled atmosphere–ocean–sea-ice–land surface model by slowly reducing the solar radiation and by increasing the planetary emissivity in the northern high latitudes. When land ice was growing, the AMOC of the zonally averaged ocean model intensified, resulting in a warm subpolar North Atlantic Ocean. A similar response is found in C115 for years 31–60 (Fig. 6a). The intensified AMOC brings more warm AW into the subpolar gyre leading to a warming here.

The idea that the AMOC increased in strength during the glacial inception finds some support from paleo observations. In the northwestern Atlantic, southeast of Newfoundland, Labeyrie et al. (1999) found increased δ^{13}C in benthic foraminifera during the period of rising benthic δ^{18}O at the transition from marine stage 5e to 5d, indicating an enhanced AMOC during the growth of the ice sheets. Furthermore, Ruddiman and McIntyre (1979) found that the subpolar North Atlantic (40°–60°N) maintained relatively warm sea surface temperatures during the major intervals of ice sheet growth.

The state of the AMOC during full glacial conditions, e.g. the last glacial maximum (LGM), is a subject of controversy, both in terms of reconstructions with paleoceanographic methods and modelling approaches. The circulation was clearly different from both the modern circulation and the model results of the present study in terms of the northward extent of warm water in the surface layer (Sarntheim et al., 2003). A shallowing of convection depth and increase in deepwater nutrient content is a consistent result of both observations and modelling (Duplessy et al., 1988; Boyle, 1995; Ganopolski et al., 1998). A number of results indicate that the main locus for overturning moved south of the Nordic Seas, but the extent to which the strength of the overturning changed is debated. Some model results indicate a reduction of up to 40% (Fichefet et al., 1994; Meissner et al., 2003), whereas others indicate a circulation close to the modern strength, but with a shallower overturning cell (Ganopolski et al., 1998). Hewitt et al. even found an intensified AMOC in their LGM simulation using a three-dimensional atmosphere–ocean GCM. The circulation in the Nordic Seas region appears very sensitive with rapid changes between different modes of operation and rapid changes in the northward extent of the AMOC (Dokken and Jansen, 1999). This indicates, as in the present

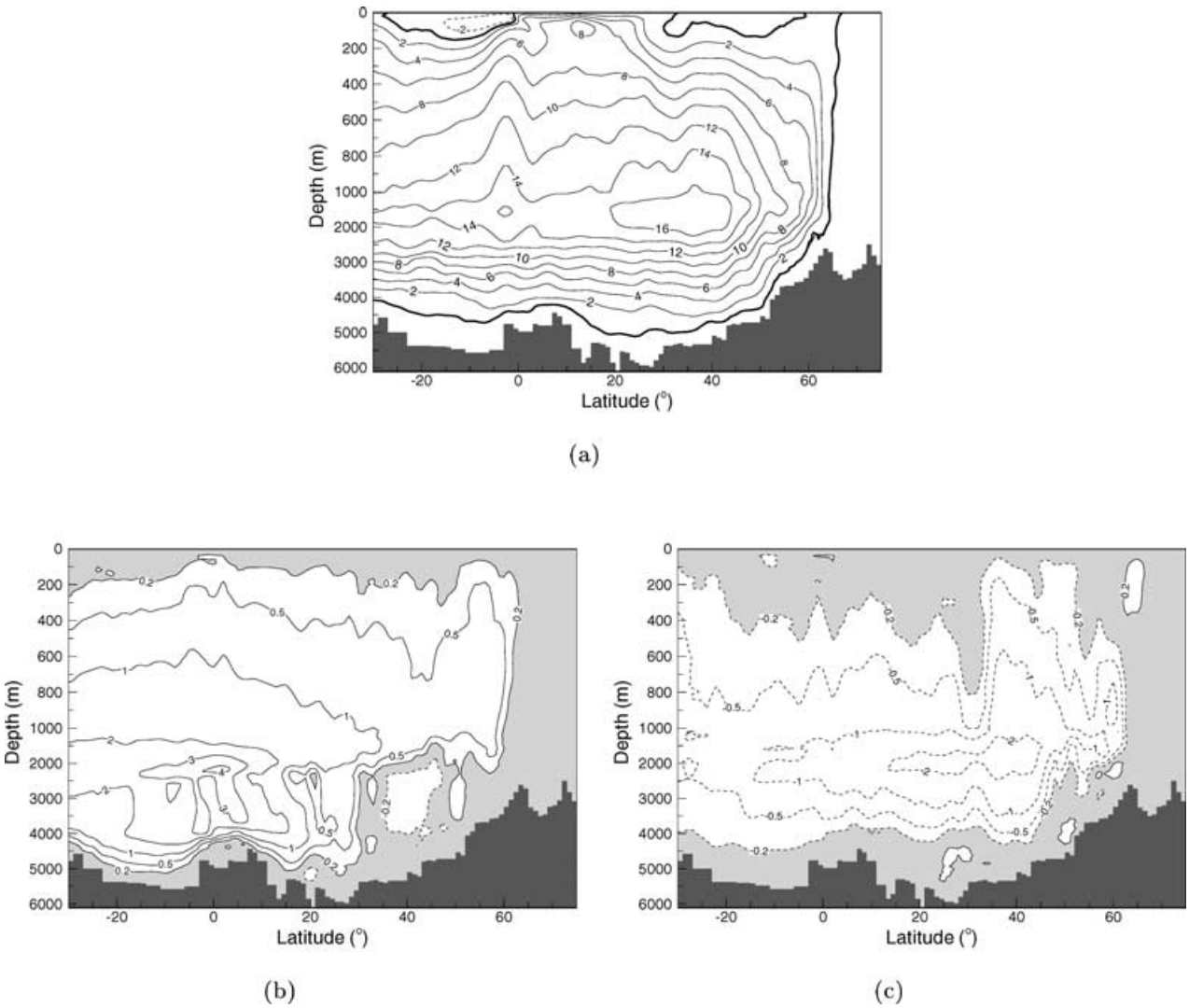

Fig. 11. (a) The annual mean AMOC stream function (Sv) for CTRL for years 31–60. Contour interval is 2 Sv. Changes in the annual mean AMOC (Sv) for years 31–60 shown as the difference C115–CTRL (b) and W125–CTRL (c). Contour interval is 1 Sv. In addition, the 0.2-Sv and 0.5-Sv contour isolines are shown.

study, that there are mechanisms in the response of the AMOC to glacial boundary conditions which at times boost the AMOC.

A possible problem with the presented simulations is related to the use of mixed boundary conditions. The model drifts in sea surface salinity and temperature are relatively small in CTRL during the 90-yr integration period (not shown). However, Rahmstorf (1995) found that important transitions in circulation can occur after more than 50 yr even if temperature and salinity drifts are slow. Furthermore, a 90-yr integration period is far too short to draw any conclusions regarding the glacial inception. Also, because the presented experiments have been conducted with an ocean-only model, this prevents any feedback from the atmosphere. For instance, the summer increase of the equator-to-pole surface temperature gradient from orbital forcing could lead to changes in the northward transport of moisture as shown by Khodri et al. (2001). This would again change the precipitation and runoff to high latitude seas and thus constitute an important atmosphere–ocean feedback. Partly because of this, Khodri et al. (2001) found a reduced AMOC of about 2 Sv in their experiment using orbital parameters for 115 kyr BP.

Nevertheless, the positive feedback on the AMOC from ocean–sea-ice interactions as found in this study is interesting, and finds some support from paleo observations and other model experiments. To assess whether or not such a feedback would be significant during glacial inceptions, more elaborate glacial inception studies using coupled atmosphere–ocean models need to be conducted. Finally, the scheme used for calculating changes in solar irradiance seems to work well in the present study, offering the possibility of applying the scheme in coupled atmosphere–ocean models at little additional cost.

5. Acknowledgments

This study has been supported by the Research Council of Norway through a personal grant to OHO, RegClim and NOClim (HD), the Program of Supercomputing, and by the G. C. Rieber Foundations. We would also like to thank Eystein Jansen and an anonymous reviewer for their helpful comments. This is publication Nr. A24 of the Bjerknes Centre for Climate Research.

References

Bentsen, M. 2002. *Modelling Ocean Climate Variability of the North Atlantic and the Nordic Seas*. PhD Thesis. Department of Mathematics, University of Bergen and Nansen Environmental and Remote Sensing Center, Bergen, Norway.

Bentsen, M. and Drange, H. 2000. Parametrizing surface fluxes in ocean models using the NCEP/NCAR reanalysis data. In: *RegClim General Technical Report No. 4*, Norwegian Institute for Air Research, Kjeller, Norway.

Bentsen, M., Evensen, G., Drange, H. and Jenkins, A. D. 1999. Coordinate transformation on a sphere using conformal mapping. *Mon. Wea. Rev.* **127**, 2733–2740.

Berger, A. and Loutre, M. F. 1991. Insolation values for the climate of the last 10 million years. *Quat. Sci. Rev.* **10**, 297–317.

Bleck, R., Dean, S., Keefe, M. O. and Sawdey, A. 1995. A comparison of data-parallell and message-passing versions of the Miami isopycnic coordinate ocean model. *Parallell Comput.* **21**, 1695–1720.

Bleck, R., Rooth, C., Hu, D. and Smith, L. T. 1992. Salinity-driven thermocline transients in a wind- and thermohaline-forced isopycnic coordinate model of the North Atlantic. *J. Phys. Oceanogr.* **22**, 1486–1505.

Boyle, E. 1995. Last-glacial-maximum North Atlantic deep water: on, off or somewhere in-between? *Phil. Trans. R. Soc. London B* **348**, 243–253.

Broecker, W. S. 1991. The great ocean conveyor. *Oceanography* **4**, 79–89.

Broecker, W. S. and Denton, G. H. 1990. What drives glacial cycles? *Sci. Am.* **262**, 49–56.

Budyko, M. I. 1969. The effect of solar radiation variations on the climate of the earth. *Tellus* **21**, 611–619.

Cortijo, E., Duplessy, J., Labeyrie, L., Leclaire, H., Duprat, J. and van Weering, T. 1994. *Eemian cooling in the Norwegian Sea and North Atlantic ocean preceding continental ice-sheet growth*. *Nature* **372**, 446–449.

Crowley, T. J. and North, G. R. 1991. *Paleoclimatology*. Oxford University Press, New York.

Dokken, T. M. and Jansen, E. 1999. Rapid changes in the mechanism of ocean convection during the last glacial period. *Nature* **401**, 458–461.

Drange, H. and Simonsen, K. 1996. *Formulation of Air–Sea Fluxes in the ESOP2 Version of MICOM*. Technical Report 125, Nansen Environmantal and Remote Sensing Center, Bergen, Norway.

Duplessy, J. C., Shackleton, N. J., Fairbanks, R. G., Labeyrie, L., Oppo, D. and Kallel, N. 1988. Deepwater source variations during the last climatic cycle and their impact on the global deepwater circulation. *Paleoceanography* **3**, 343– 360.

Fairall, C. W., Bradley, E. F., Rogers, D. P., Edson, J. B. and Young, G. S. 1996. Bulk parametrization of air–sea fluxes for Tropical Ocean–Global Atmosphere Coupled-Ocean Atmosphere Response Experiment. *J. Geophys. Res.* **101**, 3747–3764.

Fichefet, T., Hovine, S. and Duplessy, J. C. 1994. A model study of the Atlantic thermohaline circulation during the last glacial maximum. *Nature* **372**, 252–255.

Friedrich, H. and Levitus, S. 1972. An approximation to the equation of state for sea water, suitable for numerical ocean models. *J. Phys. Oceanogr.* **2**, 514–517.

Fronval, T. and Jansen, E. 1996. Rapid changes in ocean circulation and heat flux in the Nordic Seas during the last interglacial period. *Nature* **383**, 806–810.

Ganopolski, A., Rahmstorf, S., Petoukhov, V. and Claussen, M. 1998. Simulation of modern and glacial climates with a coupled global model of intermediate complexity. *Nature* **391**, 351–356.

Gaspar, P., Grégoris, Y. and Lefevre, J.-M. 1990. A simple eddy kinetic model for simulations of the oceanic vertical mixing: Tests at Station Papa and Long-Term Upper Ocean Study Site. *J. Geophys. Res.* **95**, 16 179–16 193.

Gildor, H. and Tziperman, E. 2001. A sea ice climate switch mechanism for the 100-kyr glacial cycles. *J. Geophys. Res.* **106**, 9117–9133.

Gloersen, P., Campbell, W. J., Cavalieri, D. J., Comiso, J. C. and Zwally, C. L. P. H. J. 1992. *Artic and Antarctic sea ice, 1978–1987*. National Aeronautics and Space Administration, Washington, D.C.

Harder, M. 1996. *Dynamik, Rauhigkeit und Alter des Meereises in der Arktis*. PhD Thesis. Alfred-Wegner-Institut für Polar- und Meeresforschung, Bremerhaven, Germany.

Hewitt, C. D., Stouffer, R. J., Broccoli, A. J., Mitchell, J. F. B. and Valdes, P. J. 2003. The effect of ocean dynamics in a coupled GCM simulation of the Last Glacial Maximum. *Climate Dyn.* **20**, 203–218, doi:10.1007/s00382-002-0272-6.

Hibler, W. D. 1979. A dynamic thermodynamic sea ice model. *J. Phys. Oceanogr*. **9**, 815–846.

Hilmer, M. and Lemke, P. 2000. On the decrease of Arctic sea ice volume. *Geophys. Res. Lett.* **27**, 3751–3754.

Imbrie, J., Boyle, E. A., Clemens, S. C., Duffy, A., Howard, W. R., Kukla, G., Kutzback, J., Martinson, D. G., McIntyre, A., Mix, A. C., Morley, B. M. J. J., Peterson, L. C., Pisias, N. G., Prell, W. L., Raymo, M. E., Shackleton, N. J. and Toggweiler, J. R. 1992. On the structure and origin of major glaciation cycles. 1. Linear responses to Milankovitch forcing. *Paleoceanography* **7**, 701–738.

Khodri, M., Leclainche, Y., Ramstein, G., Braconnot, P., Marti, O. and Cortijo, E. 2001. Simulating the amplification of orbital forcing by ocean feedbacks in the last glaciation. *Nature* **410**, 570–574.

Kutzbach, J. E. and Gallimore, R. G. 1988. Sensitivity of a coupled atmosphere/ML ocean model to changes in orbital forcing at 9000 years BP. *J. Geophys. Res.* **93**, 803–821.

Labeyrie, L., Leclaire, H., Waelbroeck, C., Cortijo, E., Duplessy, J. C., Vidal, L., Elliot, M., Coat, B. L. and Auffret, G. 1999. Temporal variability of the surface and deep waters of the North West Atlantic Ocean at orbital and millennial scales. In: *Mechanisms of Global Climate Change at Millennial Time Scales* (eds. P. U. Clark, R. S. Webb and L. D. Keigwin), Vol. 112 of *Geophysical Monograph*. American Geophysical Union, Washington, D.C.

Lambert, S. J. and Boer, G. J. 2001. CMIP1 evaluation and intercomparison of coupled climate models. *Climate Dyn.* **17**, 83–106.

Levitus, S. and Boyer, T. P. 1994. *World Ocean Atlas 1994, Volume 4: Temperature*. NOAA Atlas NESDIS 4, Washington, D.C., 117 pp.

Levitus, S., Burgett, R. and Boyer, T. P. 1994. *World Ocean Atlas 1994, Volume 3: Salinity*. NOAA Atlas NESDIS 3, Washington, D.C., 99 pp.

Meissner, K. J. and Gerdes, R. 2002. Coupled climate modelling of ocean circulation changes during ice age inception. *Climate Dyn.* **18**, 455–473.

Meissner, K. J., Schmittner, A., Weaver, A. J. and Adkins, J. F. 2003. Ventilation of the North Atlantic Ocean during the Last Glacial Maximum: A comparison between the simulated and observed radiocarbon ages. *Paleoceanography* **18**, 1023, doi:10.1029/2002PA000762.

Mikolajewicz, U. and Maier-Reimer, E. 1994. Mixed boundary conditions in ocean general circulation models and their influence on the stability of the model's conveyor belt. *J. Geophys. Res.* **99**, 22633–22644.

National Oceanic and Atmospheric Administration (NOAA). 1988. *Data Announcement 88-MGG-02, Digital relief of the surface of the Earth*. Technical report, NOAA, National Geophysical Data Center, Boulder, CO, USA.

Rahmstorf, S. 1995. Climate drift in an ocean model coupled to a simple, perfectly matched atmosphere. *Climate Dyn.* **11**, 447–458.

Rahmstorf, S. 1999. Decadal variability of the thermohaline circulation. In: *Beyond El Ninõ* (ed.A. Navarra). Springer-Verlag, Berlin.

Ruddiman, W. F. and McIntyre, A. 1979. Warmth of the subpolar north Atlantic Ocean during northern hemisphere ice-sheet growth. *Science* **204**, 173–175.

Sarntheim, M., Gersonde, R., Niebler, S., Pflaumann, U., Spielhagen, R., Thiede, J., Wefer, G. and Weinelt, M. 2003. Overview of Glacial Atlantic Ocean Mapping (GLAMAP 2000). *Paleoceanography* **18**, 1030, doi:10.1029/2002PA000769.

Wang, Z. and Mysak, L. A. 2000. A simple coupled atmosphere–ocean–sea-ice–land surface model for climate and paleoclimate studies. *J. Climate* **13**, 1150–1172.